Open access • Journal Article • DOI:10.1002/2016GC006657

Lithospheric structure of Iberia and Morocco using finite-frequency Rayleigh wave tomography from earthquakes and seismic ambient noise — Source link

Imma Palomeras, Antonio Villaseñor, S. Thurner, Alan Levander ...+2 more authors

Institutions: Rice University, Spanish National Research Council

Published on: 01 May 2017 - Geochemistry Geophysics Geosystems (John Wiley & Sons, Ltd)

AGU PUBLICATIONS

Geochemistry, Geophysics, Geosystems

RESEARCH ARTICLE
10.1002/2016GC006657

Key Points:
- 3-D Shear velocity model of Iberia and north Morocco
- Moho and LAB map of Iberia and north Morocco
- Crustal and Upper mantle imaging

Correspondence to:
I. Palomeras,
imma@usal.es

Citation:
Palomeras, I., A. Villaseñor, S. Thurner, A. Levander, J. Gallart, and M. Harnafi (2017), Lithospheric structure of Iberia and Morocco using finite-frequency Rayleigh wave tomography from earthquakes and seismic ambient noise, *Geochem. Geophys. Geosyst.*, *18*, 1824–1840, doi:10.1002/2016GC006657.

Received 20 SEP 2016
Accepted 13 MAR 2017
Accepted article online 28 MAR 2017
Published online 4 MAY 2017

Lithospheric structure of Iberia and Morocco using finite-frequency Rayleigh wave tomography from earthquakes and seismic ambient noise

I. Palomeras[1,2], A. Villaseñor[3], S. Thurner[1], A. Levander[1], J. Gallart[3], and M. Harnafi[4]

[1]Rice University, Houston, Texas, USA, [2]Department of Geology, University of Salamanca, Salamanca, Spain, [3]Institute of Earth Sciences Jaume Almera, ICTJA-CSIC, Barcelona, Spain, [4]Scientific Institute of Rabat, Université Mohammed V-Agdal, Rabat, Morocco

Abstract We present a new 3-D shear velocity model of the western Mediterranean from the Pyrenees, Spain, to the Atlas Mountains, Morocco, and the estimated crustal and lithospheric thickness. The velocity model shows different crustal and lithospheric velocities for the Variscan provinces, those which have been affected by Alpine deformation, and those which are actively deforming. The Iberian Massif has detectable differences in crustal thickness that can be related to the evolution of the Variscan orogen in Iberia. Areas affected by Alpine deformation have generally lower velocities in the upper and lower crust than the Iberian Massif. Beneath the Gibraltar Strait and surrounding areas, the crustal thickness is greater than 50 km, below which a high-velocity anomaly (>4.5 km/s) is mapped to depths greater than 200 km. We identify this as a subducted remnant of the NeoTethys plate referred to as the Alboran and western Mediterranean slab. Beneath the adjacent Betic and Rif Mountains, the Alboran slab is still attached to the base of the crust, depressing it, and ultimately delaminating the lower crust and mantle lithosphere as the slab sinks. Under the adjacent continents, the Alboran slab is surrounded by low upper mantle shear wave velocities (Vs < 4.3) that we interpret as asthenosphere that has replaced the continental margin lithosphere which was viscously removed by Alboran plate subduction. The southernmost part of the model features an anomalously thin lithosphere beneath the Atlas Mountains that could be related to lateral flow induced by the Alboran slab.

1. Introduction and Tectonic Setting

The westernmost Mediterranean comprises the Iberian Peninsula and Morocco, separated by the Alboran Sea and the Algerian Basin (Figure 1). This area, the far western end of the Alpine-Himalayan orogenic belt, is currently affected by the Africa-Eurasia convergence with deformation extending from the Pyrenees in the north of Iberia to the Atlas Mountains in Morocco. The current convergence rate is ~3 mm/yr with Iberia moving to the southwest relative to Africa [e.g., *Koulali et al.*, 2011].

A series of tectonic events have affected this area since the Paleozoic. From late Ordovician to the Permian, different continental blocks were accreted to form the supercontinent Pangaea. The Variscan orogeny resulted from the collision of Baltica-Laurentia and Gondwana in Devonian to Carboniferous times [*Matte*, 1986]. During continental convergence, the Armorica and Avalonia microplates docked against Baltica-Laurentia in the active margin with Gondwana [*Matte*, 2001]. In Iberia, this orogeny is represented by the Iberian Massif which outcrops in almost the entire western half of the peninsula (Figure 1a). In Africa, Variscan age Gondwanan rocks are found in the Moroccan Meseta, the Anti-Atlas, and the Sahara craton. During the Mesozoic, Pangaea broke up as the Neo-Tethys Ocean opened from east to west, separating the future Eurasian plate from Africa. Breakup included formation of rift grabens and basins in both northern Africa and Iberia. Iberia became a microplate surrounded by shallow waters and sedimentary basins. In the Middle Jurassic to early Cretaceous, the Atlantic opened to the west of Iberia, with the Iberian plate rotating counter-clockwise and opening the Bay of Biscay. Initiation of African-Eurasian convergence in the Cretaceous accreted Iberia to the Eurasian plate forming the Pyrenees. Continued African-Eurasian convergence is thought to have transmitted the plate margin stress fields that reached the interior of the Iberian plate, forming a thrust system on the previous Mesozoic rift basins, creating, e.g., the Iberian Chain. The

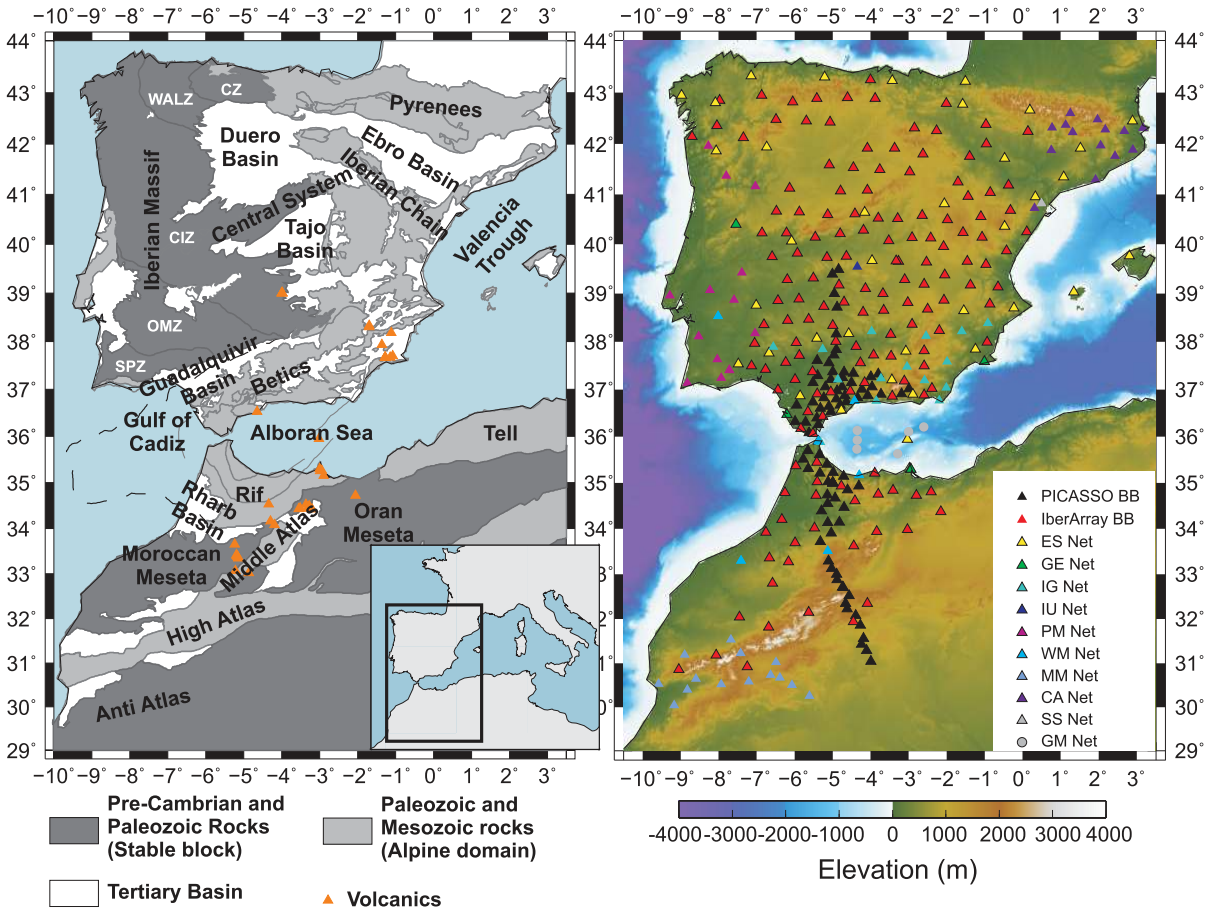

Figure 1. (a) Tectonic map of the Western Mediterranean. Orange triangles represent the Cenozoic volcanic fields. The Iberian Massif terranes have been named: SPZ: South Portuguese Zone; OMZ: Ossa-Morena Zone; CIZ: Central Iberian Zone; WALZ: West Asturian-Leonese Zone; CZ: Cantabrian Zone. (b) Topographic map with the broadband stations used in this study. Color codes are used to signify different arrays (inset).

topography of the Central System and that of the Cantabrian Mountains together with their foreland basins, the Duero and Tajo tertiary basins were also formed during this time. In North Africa, a Mesozoic Rift System was inverted and uplifted since the Middle Eocene, forming the Atlas Mountains [*Jacobshagen et al.*, 1988; *Laville et al.*, 2004]. Cenozoic African-European convergence resulted in subduction of the Tethys oceanic plate beneath parts of southern Europe. The subduction zone against northeastern Spain began to retreat rapidly starting at 30–25 Ma, separating into multiple segments as it traversed eastward toward Italy and southward to Africa, forming the modern western Mediterranean basins [*Royden*, 1993; *Rosenbaum et al.*, 2002; *Chertova et al.*, 2014; *Van Hinsbergen et al.*, 2014]. One of these segments moved southwestward, opening the Algerian and Alboran basins. The retreating trench reached the passive margins of south Iberia and north Morocco in the Middle-Late Miocene, initiating construction of the Betics-Rif fold and thrust belts and their foreland basins, the Guadalquivir in Iberia and the Rharb in Morocco [*Rosenbaum et al.*, 2002; *Van Hinsbergen et al.*, 2014].

Neogene volcanic fields are found in northeastern Iberia (Catalan Volcanic Province, CVP), the Valencia Trough, the eastern Betics and Rif, the Alboran Sea, the isolated Calatrava Volcanic Field (CVF) north of the Betics, and are widespread in the Middle and High Atlas. All these volcanics, except the CVF and the ones in the Atlas, show a similar evolution from silica rich magmas in the Early to Middle Miocene, to silica poor magmas from the Late Miocene to present [e.g., *Martí et al.*, 1992; *Duggen et al.*, 2005]. The change in composition indicates a shift from calc-alkaline subduction-related volcanism to asthenosphere sourced melts. The geochemistry of the CVF and the Atlas volcanic provinces indicates their alkaline magmas have a subcontinental lithospheric origin [e.g., *Cebriá and López-Ruiz*, 1995; *Bosch et al.*, 2014].

Following the terminology of *Gibbons and Moreno* [2002] for Spain, Iberia, and Morocco can be divided into (1) Variscan zones consisting of the largely stable Iberian Massif and Moroccan Meseta, where Paleozoic rocks outcrop and (2) the Cenozoic Alpine zones of eastern and southern Iberia, and those from Morocco (the Rif and Atlas Mountains) (Figure 1a). Currently the western Mediterranean is under compressive deformation due to the convergence between Eurasia and Africa. Active deformation is distributed over the Betic-Rif chain, Gulf of Cadiz, and Alboran Sea as a diffuse band [*Buforn and Udias*, 2010] with high seismic activity in the crust and at intermediate depths, and a few deep events at ~650 km depth beneath Granada [e.g., *Buforn et al*., 1991]. Local tectonics in this region are complicated with extension occurring in the eastern Betics and Rif, compression to the west, and strike slip on the Trans Alboran Shear Zone (TASZ) [*Stich et al*., 2006]. The active region is surrounded by the less deformed Variscan zone in Iberia and by the Sahara Craton to the south of the Atlas Mountains.

Body wave tomography studies have imaged a high-velocity anomaly beneath the westernmost Mediterranean that has been interpreted as the remnant of trench rollback of the Alboran slab [*Blanco and Spakman*, 1993; *Calvert et al*., 2000; *Gutscher et al*., 2002; *Garcia-Castellanos and Villaseñor*, 2011; *Bezada et al*., 2013]. Recent active and passive seismic studies of the lithosphere have identified unusually thick crust under the western Betics and Rif [*Gil et al*., 2014; *Palomeras et al*., 2014; *Thurner et al*., 2014] and imaged crustal delamination beneath the central Betics and Rif [*Palomeras et al*., 2014; *Thurner et al*., 2014] in response to the Alboran slab subduction. Lithosphere thickness variations suggest that the subducting Alboran slab viscously thins the adjacent continental margin lithosphere mantle [*Levander et al*., 2014].

Our goal in this paper is to present an improved lithosphere and asthenosphere shear velocity model of the western Mediterranean from the Pyrenees to the Sahara craton, using Rayleigh wave phase velocity dispersion. We used the extensive data set available from recent experiments and permanent networks. The availability of this dense array data provides a unique opportunity to obtain high-resolution images of the western Mediterranean lithosphere.

2. Data and Methodology

We used data from 368 broadband seismic stations of permanent and temporary arrays deployed in the area (Figure 1b). Permanent networks included those of Morocco, Spain, and Portugal. Temporary arrays included the recent IberArray (2007–2013, Spain), PICASSO (2009–2012, USA), Münster University (2010–2012, Germany), and Bristol University (2010–2012, UK) experiments. Average interstation spacing is approximately 60 km (Figure 1b) with almost uniform coverage across Iberia and northern Morocco, but less regular coverage in the Middle and High Atlas Mountains. To obtain a velocity model from the surface to ~200 km depth, we did Rayleigh wave tomography using both ambient noise and teleseismic earthquakes.

2.1. Ambient Noise Tomography

We have obtained phase velocity maps of fundamental mode Rayleigh waves between 4 and 40 s from cross correlation of seismic ambient noise. To obtain the maps presented here we followed the approach used by *Silveira et al*. [2013]. The main difference with respect to these authors is that we have used a longer time period to compute the stacked cross correlations (2008–2011), and a much larger data set that included 350 of the broadband stations described previously.

The first step for ambient noise tomography is the determination of empirical Green's functions by cross correlating and stacking continuous recordings of all the potential station pairs. We follow the procedure of *Bensen et al*. [2007]: first, we extracted 4 h time windows from the continuous recording, eliminating those that contained 2 or more data gaps, filled the remaining gaps with the average of the signal before and after the gap, converted all the records to velocity, and decimated them to five samples per second. In order to avoid the contamination of the noise recordings by earthquakes and nonstationary sources near the stations, we have applied a "temporal normalization" by dividing the noise signal by the running average (with a width of 256 s) of the absolute value of the waveform amplitude filtered between 20 and 100 s (the dominant period band of the earthquake surface wave energy). Then we have applied spectral normalization or "whitening" to correct for the fact that the ambient noise amplitude spectrum is not flat in the potential period band of interest (e.g., 1–50 s). This is achieved by dividing the true amplitude spectrum of each noise window by the smoothed amplitude spectrum. Finally, with the objective of improving the signal-to-noise

ratio, all the processed recordings are cross correlated and stacked for the entire common time period available to each station pair.

The empirical Green's functions constructed using this methodology contain causal and acausal Rayleigh waves (in positive and negative times, respectively). To measure phase velocities we calculated the symmetric cross correlation by averaging the causal and acausal segments (reversing the time for the latter). Phase velocity dispersion is then measured using an automated implementation of the frequency-time analysis (FTAN) methodology [*Levshin et al*., 1992]. Following *Bensen et al*. [2007], from the complete set of measurements we have selected for tomography those phase velocity measurements that have values of signal-to-noise ratio (SNR) $>$ 10.

Finally, we applied a finite-frequency tomographic inversion [*Barmin et al*., 2001] to the selected phase velocity measurements between 4 and 40 s periods to obtain fundamental-mode Rayleigh-wave phase velocity maps on a 0.5° $\times$ 0.5° grid across the study area. The tomography method of *Barmin et al*. [2001] approximately accounts for the spatially extended frequency-dependent sensitivity of the waves by using Gaussian sensitivity kernels.

2.2. Teleseismic Surface-Wave Tomography

We analyzed 168 teleseismic events occurring between April 2009 and December 2011 with magnitudes greater than 6.0 and epicentral distances between 30° and 120° that were recorded by a large fraction of the 368 available broadband stations. Not all the stations recorded the entire time period as the IberArray stations were relocated as part of the operational plan [*Díaz et al*., 2009]. The path density is high at all periods (Figure 2b), and the azimuthal distribution of events is good, with the largest number of events coming from the northeast and the lowest from the SSE (Figure 2a).

We analyzed the vertical component Rayleigh wave signals. The seismograms were corrected for instrument response, and filtered with 18 Butterworth band-pass filters in the period band of 20–167 s (20, 22, 25, 27, 30, 34, 40, 45, 50, 59, 67, 77, 87, 100, 111, 125, 143, and 167 s). The fundamental mode Rayleigh wave is isolated from other modes and body waves by windowing filtered records with a variable length tapered window. The amplitude was corrected for frequency-dependent anelastic attenuation and geometrical spreading [*Mitchell*, 1995] and normalized to the root mean square amplitude for each event.

The 2-D phase velocity for periods from 20 to 167 s was calculated using the modified two-plane wave technique as described by *Forsyth and Li* [2005] with 2-D finite-frequency kernels for both amplitude and phase [*Yang and Forsyth*, 2006]. To preserve the plane wave assumption, the study area was divided into two regions. The northern region comprises the Iberian Peninsula while the southern one comprises the Betics, the Alboran Sea, and the Atlas mountains (Figure 2b). The phase velocities of the southern region are described in *Palomeras et al*. [2014]. We followed the same procedure and parameters to obtain the phase velocity for the northern region. Although the difference between the calculated phase velocities in the overlapping portions (from $-$10° to 0.5° in longitude and from 35° to 42° in latitude) is not greater than 0.10 km/s in most of the periods and points, decreasing to less than 0.05 km/s to larger periods, the phase velocities were merged using a weighted averaging function. At the northern edge of the southern box, the weight is zero, and increases linearly to one moving south. The same weighting is applied to the northern region increasing from zero to one as we move north. Both areas have the same weight value (0.5) at the central point of the overlap.

3. Phase Velocity Maps

The phase velocity maps (Figure 3) from both the ANT and the teleseismic Rayleigh waves show higher values in Variscan Iberia than in Alpine Iberia at short periods (4–35 s and 25–40 s, respectively). These results image the consequences that the age of tectonic events and the orogenic evolution of the Iberian Peninsula have in its crustal structure. We observe unusually low-phase velocities beneath Gibraltar from 4 to 50 s suggesting a thick crust. Low-phase velocities are also found in the eastern end of the Rif and the Betics, and beneath the Middle and High Atlas in the period range 40 s up to 87 s. These periods typically sample the lowermost crust and uppermost mantle.

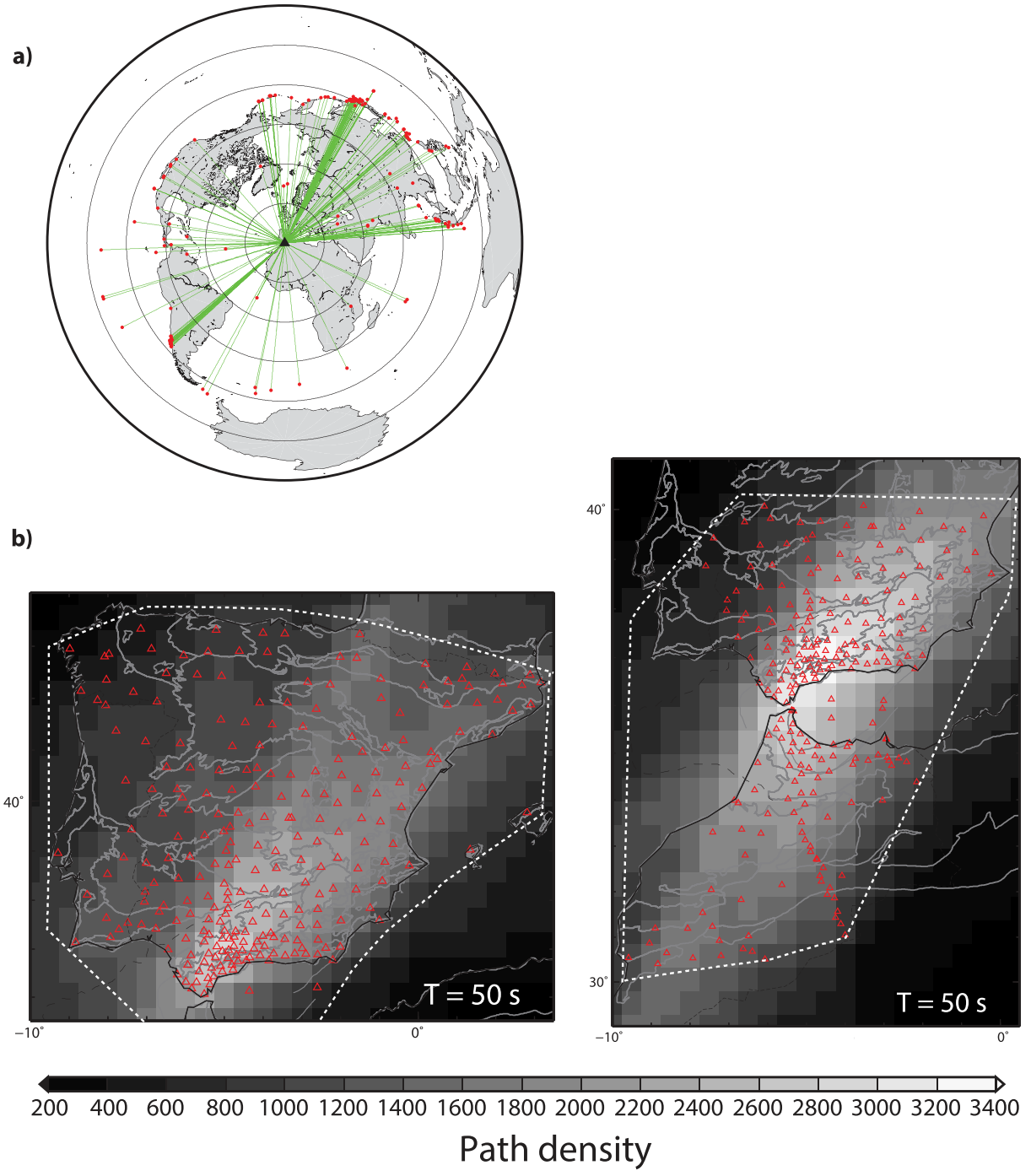

Figure 2. (a) Azimuthal distribution of earthquakes (red dots) used in this study. (b) Ray coverage shown as a gray scale for 50 s period in the two regions into which the study area has been divided (see text). Open red triangles are the stations used in this study. White dashed lines outline the areas with good ray coverage, those with at least 1400 hits.

4. Inversion

The ANT and teleseismic phase velocities data sets were calculated on a regular 0.5° × 0.5° grid and overlap in periods from 20 to 40 s. To obtain the final dispersion curves from 4 to 167 s, we averaged the phase velocity for the overlapping periods (25–35 s) at each grid node. Following *Yao et al.* [2008], we averaged the phase velocities, and found all overlapping phase velocities differed by less than 0.15 km/s. Actually, the 80% of the phase velocities differ less than 0.10 km/s. At 20 s, we used the values obtained from ANT and at

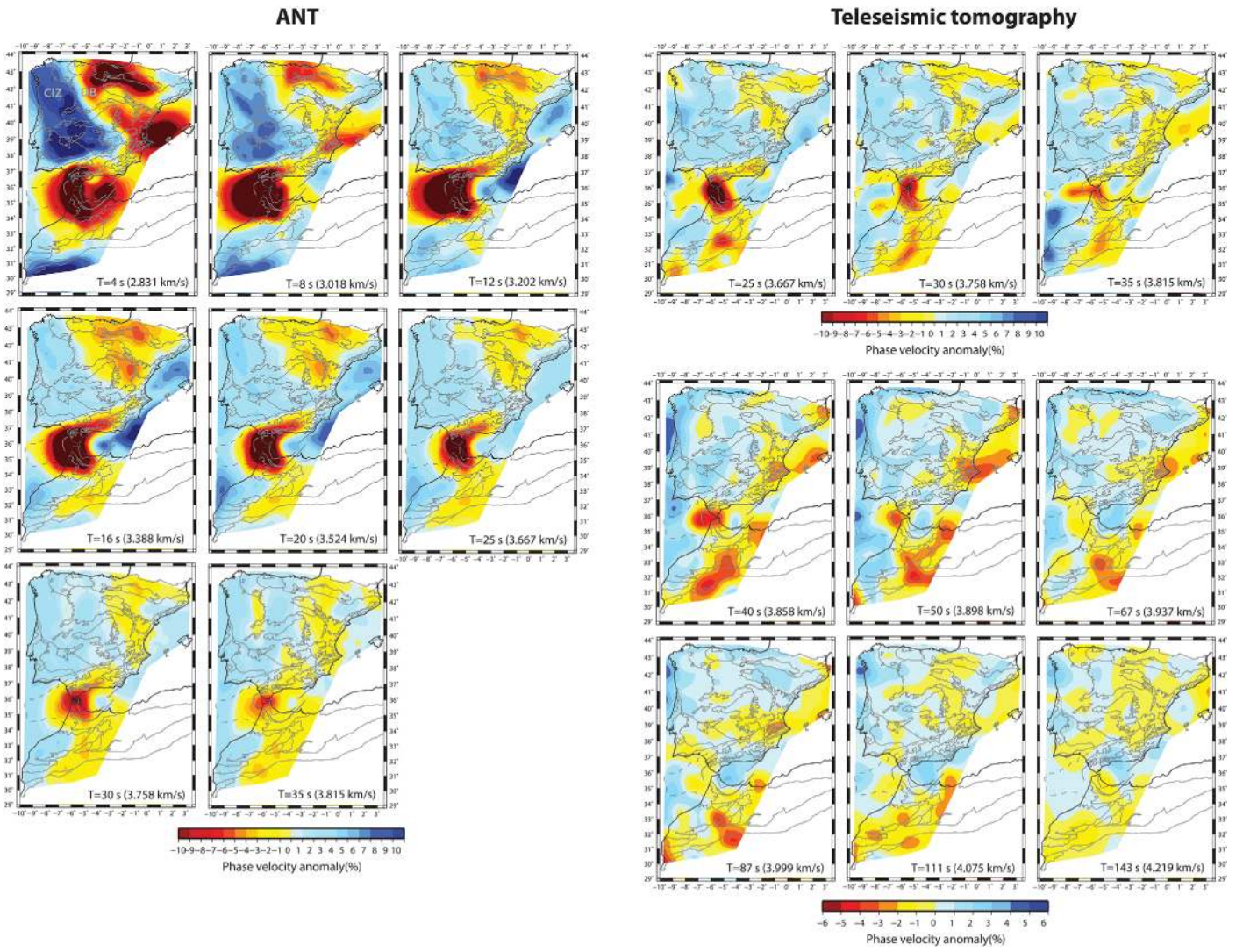

Figure 3. (left plots) Rayleigh wave phase velocity maps for the ambient noise tomography (ANT) and (right plots) the ballistic finite-frequency tomography. The plotted phase velocity anomaly is referred to the average phase velocity at each period. The area with no ray coverage (see Figure 3b) is masked. CIZ: Central Iberian Zone; DB: Duero Basin.

40 s the ones obtained from the earthquake tomography. The resulting dispersion curves (Figure 4a) have been inverted on a node-by-node basis using the surface wave code from the Computational Programs in Seismology package [*Herrmann*, 2013]. We ran 30 iterations at each grid node with a starting Vs model that consists of a homogenous layer with velocity Vs = 4.4 km/s down to 200 km depth. From there velocity increases progressively with depth as in AK135 model [*Kennett et al*., 1995] (Figure 4b). We fixed the Vp/Vs ratio in each layer also using the AK135 model Vp/Vs ratios, allowing for variations in Vs and Vp.

5. Results

5.1. Crust

The shear velocity model we obtained shows lateral variations that conform well with tectonic and geologic features (Figures 5 and 6). At shallow depths (<8 km), the highest shear velocities (>3.2 km/s) are observed in the Variscan Iberia, where Paleozoic rocks outcrop. Lower velocities (<3.0 km/s) are obtained in the Alpine belts both in Iberia and North Africa. The lowest shear velocities (<2.4 km/s) at shallow depths are observed beneath the Gibraltar Strait and Gulf of Cadiz. There, velocities much lower than elsewhere persist to 50 km depth. Somewhat higher, but still low velocities are also found in the crust under the Betics and Rif at all depths to 45 km.

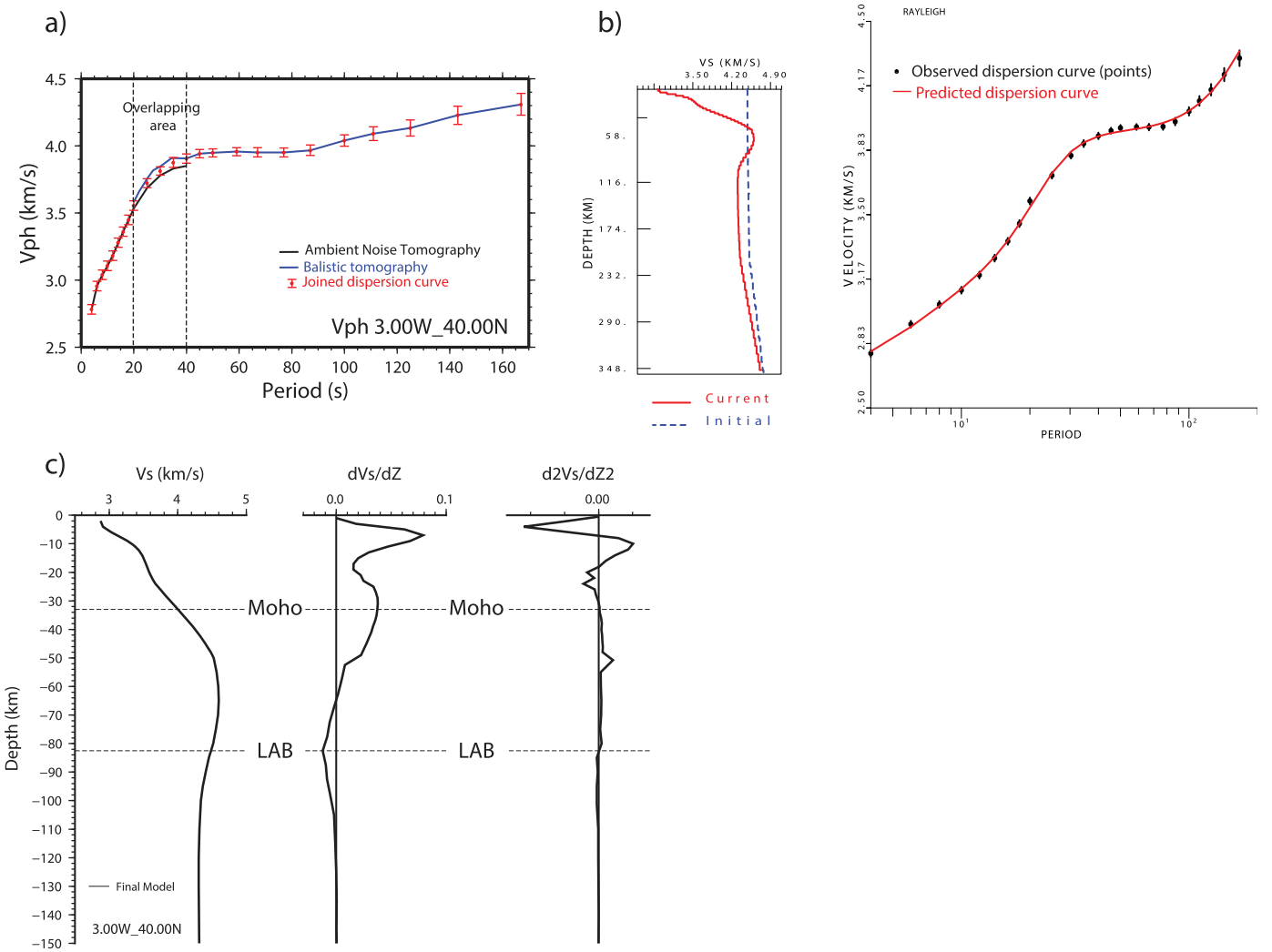

Figure 4. All figures are for grid node 3.00–40.00 W. (a) Dispersion curve to invert to obtain the shear velocity (red dots) averaged from the ambient noise tomography (black line) and the ballistic tomography (blue line) for the periods between 20 and 40 s. (b) (left plot) 1-D shear velocity model after inversion (red line) and (right plot) predicted dispersion curve (red line). Blue dashed line is the initial shear velocity model and dots are the phase velocities. (c) Final 1-D velocity model, with its first and second derivatives. The Moho and LAB depths predicted from the maximum d*V*/d*z* and minimum d2*V*dz2, respectively, are labeled. See text for explanation.

At middle crustal depths (15 km depth), the contrast between the Variscan and Alpine areas decreases and shear velocity differences are less obvious, with values of ~3.5 km/s. In the Gibraltar Strait velocities are still considerably lower (~2.6 km/s) than elsewhere.

From 20 km depth and greater (e.g., ~45 km in the Pyrenees), the Alpine belts have lower crustal velocities than either the Iberian Massif or the Tertiary basins, either in Iberia and Morocco. This implies important differences in the Moho depth. As noted above the lowest deep crust velocities occur in the Gibraltar Strait, Rif Mountains, and eastern Betics.

5.2. Upper Mantle

The most obvious feature observed in the upper mantle is a high shear velocity body beneath the Alboran Domain, western Betics, and northwestern Rif, emerging at ~50 km depth and extending to the bottom of the model at ~230 km depth (Figures 5 and 6). This high-velocity body has very low to moderately low shear velocities (4.1–4.2 km/s) around it, depending on depth. The lowest shear velocities in the upper mantle are observed beneath the High and Middle Atlas, and in the area east of the Betics extending through the Valencia trough and to the northeastern coast of Iberia. Another region of low upper mantle shear

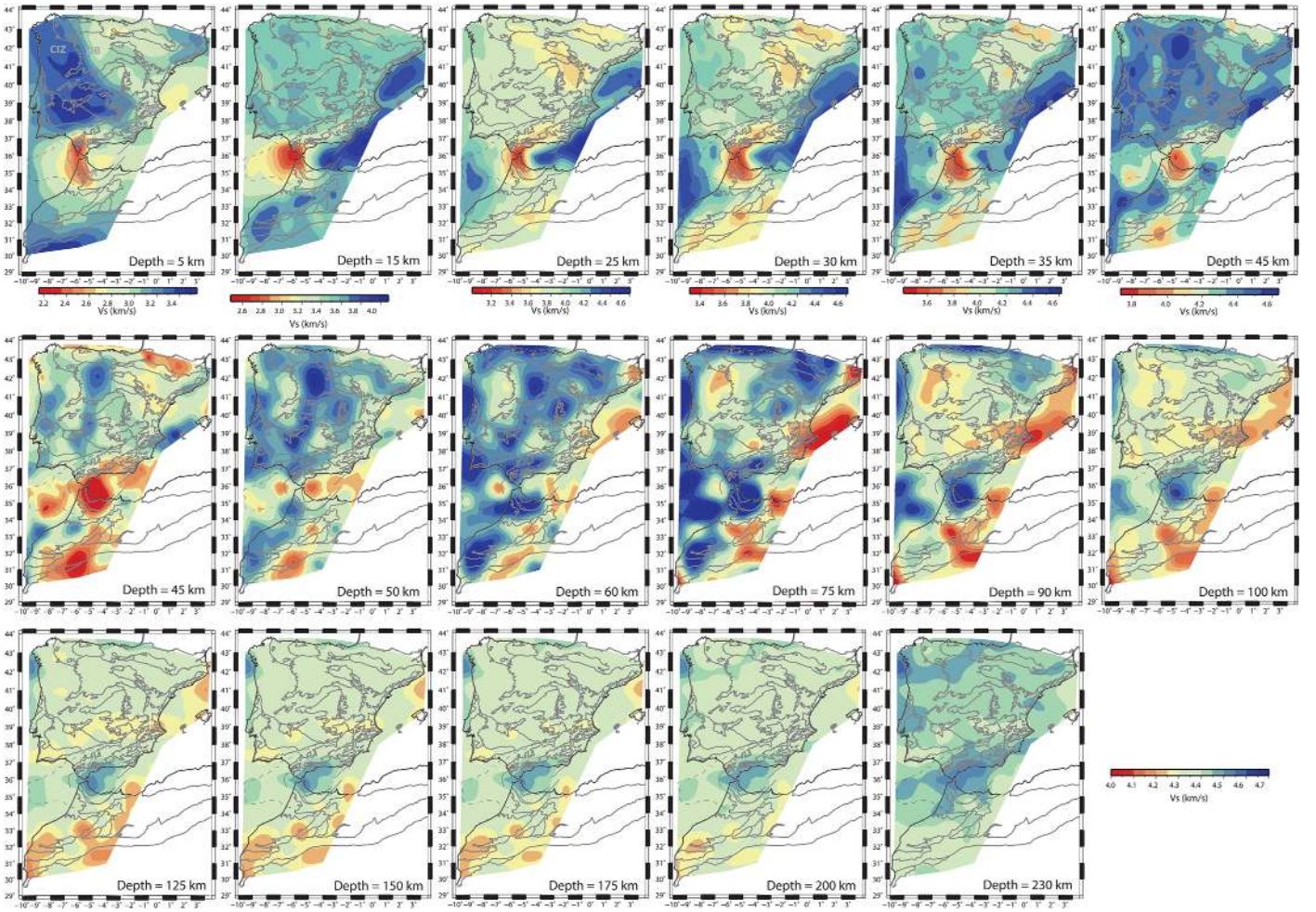

Figure 5. Maps of absolute shear velocity at different depths. (top plots) A different color scale is used for each crustal depth. A common color scale is used for upper mantle depths. The area with no ray coverage (see Figure 3b) is masked. CIZ: Central Iberian Zone; DB: Duero Basin.

velocity extends from 50 to 100 km depth in the Central Iberian Zone (CIZ) at the boundary between the Duero Basin and the Iberian Massif.

5.3. Crustal and Lithospheric Thickness

Surface wave analysis is sensitive to the variation of absolute seismic velocities with depth but as it averages over depth ranges it is relatively insensitive for finding the exact depths of impedance discontinuities. Although surface wave tomography is not capable of distinguishing between a sharp velocity contrast or a gradual velocity gradient, many authors use different criteria to estimate the depth to the seismic lithosphere-asthenosphere boundary (LAB) from surface waves observations [*Eaton et al*., 2009]. One proxy is to take the depth of the strongest negative velocity gradient (first derivative with respect to depth) at the base of the high-velocity mantle lid [e.g., *Li et al*., 2003; *Priestley and Debayle*, 2003]. Along these lines we determined the crustal and the lithospheric thickness from taking the vertical derivative of the 1-D shear velocity profiles at each gridpoint (Figure 4c). The Moho is selected as the depth of the maximum positive gradient having a shear velocity greater than 4.0 km/s while the LAB depth is chosen as the minimum of the first derivative at depths greater than 40 km. To estimate the accuracy of the method, we created a synthetic dispersion curve from a 1-D shear velocity model with a Moho and LAB at 40 km and 100 km depth, respectively. We have also added uncertainty at each period as the averaged uncertainty of the real data. Then we inverted the dispersion curve using as initial model the one used to create the synthetic curve (Figure 7a) and using the same 1-D shear velocity model used to invert the data presented in this manuscript (Figure 7b). Afterward, we calculated the first and second derivative of the final model. The Moho and LAB

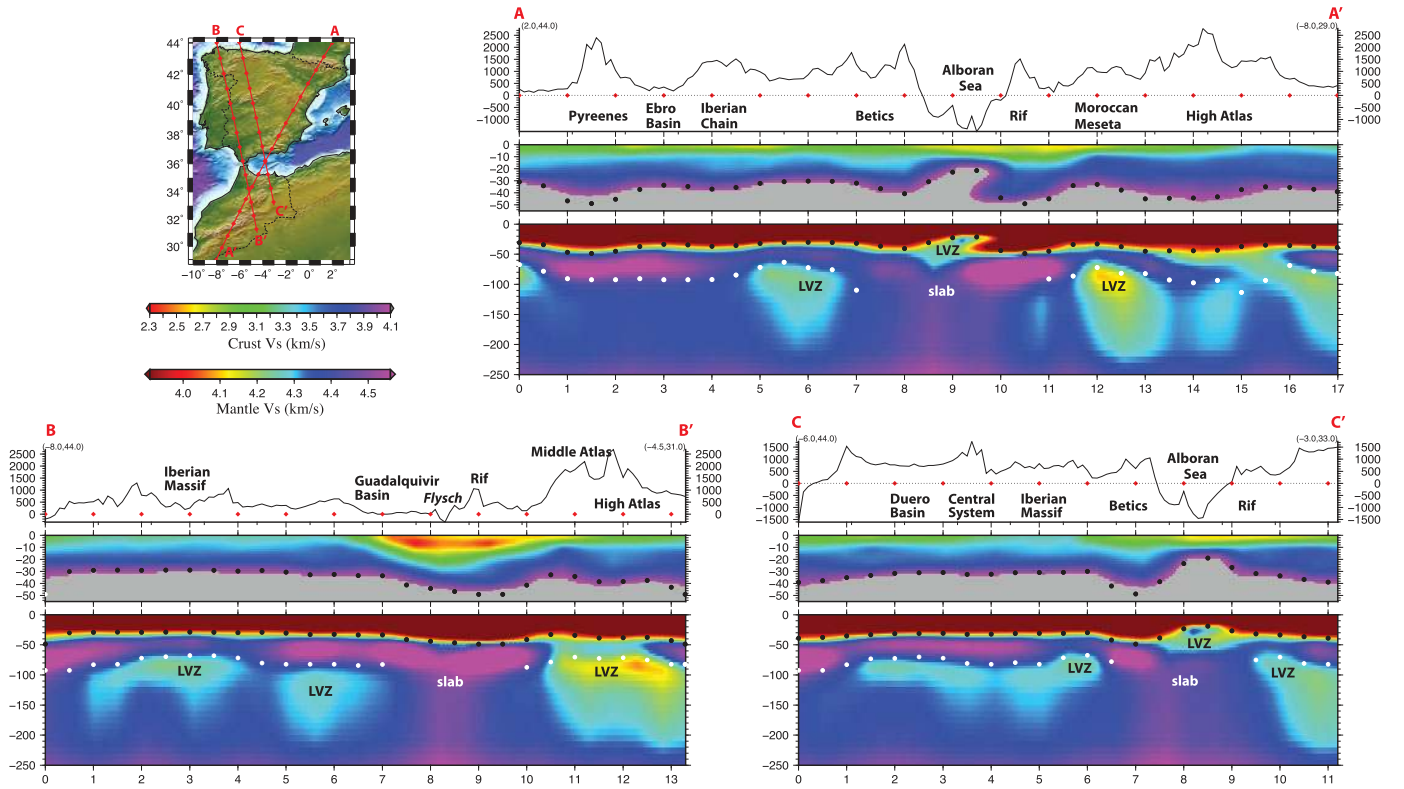

Figure 6. Absolute shear velocity cross sections. Sections cross the different tectonic provinces showing lateral variations in the shear velocities. (top plot) The topography. Middle plot shows the crustal shear velocities and bottom plot the upper mantle shear velocities. Distance is in great arc degrees. Black dots indicate the calculated Moho depth and white dots the LAB depth (see text for explanation). The low upper mantle velocity areas are also marked, as well the high velocities that are interpreted as the Alboran Slab.

depths are estimated as the maximum and minimum on the first derivative, respectively, and as zeros in the second derivative (Figure 7c). The recovered and the real Moho and LAB have some discrepancies. The differences are approximately 2 km thick for the Moho and approximately 6 km for the LAB (red dashed lines in Figure 7c). Therefore, we estimate that the maximum error in depth is ±2 km for the Moho and ±6 km for the LAB. (Other possible errors are those associated with the irregular azimuthal sampling, and errors in calculating the phase velocities. However, the consistency of the trends in a model created from the 1-D velocity profiles and the fact that Moho and LAB depths are determined from gradients and not absolute velocities suggest little influence of the above mentioned factors.)

The Moho depth map for Iberia (Figure 8a) presents a thick crust (∼50 km) beneath the Pyrenees that does not extends to the west toward the Cantabrian Chain as was suggested by other authors [e.g., *Díaz and Gallart*, 2009]. Our results show a shallower Moho (32 km) west of the Pyrenees that deepens to 38 km under the Cantabrian Chain. We also observe thick crust beneath the Iberian Chain (∼38 km) and the Ebro Basin (∼36 km). South of the Iberian Chain, to the east of the Betics (the PreBetics), the Moho shallows to 26–27 km. Moho depth in the Valencia trough is less than 20 km.

The distinction between Variscan and Alpine Iberia is also reflected in crustal thickness. The Variscan crust is overall thinner than Alpine Iberia, averaging 31 km versus 36 km. Beneath northwestern Variscan Iberia, in the Central Iberian Zone, the Moho is at 29–30 km. The Moho deepens to 32 km at the southern part of the Iberian Massif. We estimate a Moho depth of approximately 50 km under the Gibraltar Arc (western Betic and Rif mountains and the Gibraltar Strait). This deep Moho is consistent with Moho depths determined from receiver functions (RF) analysis [*Mancilla et al.*, 2012; *Thurner et al.*, 2014] and a wide-angle seismic experiment in the Rif [*Gil et al.*, 2014]. For the Alboran Sea, we found a crustal thickness of ∼18 km.

For the Middle and High Atlas, we obtained a crustal thickness of 34 km thickening to 38 km south of the Middle Atlas and to 30 km to the north. This agrees with the Moho depths obtained with an active seismic experiment [*Ayarza et al.*, 2014]. Deeper Moho (∼48 km) is observed for the western Atlas.

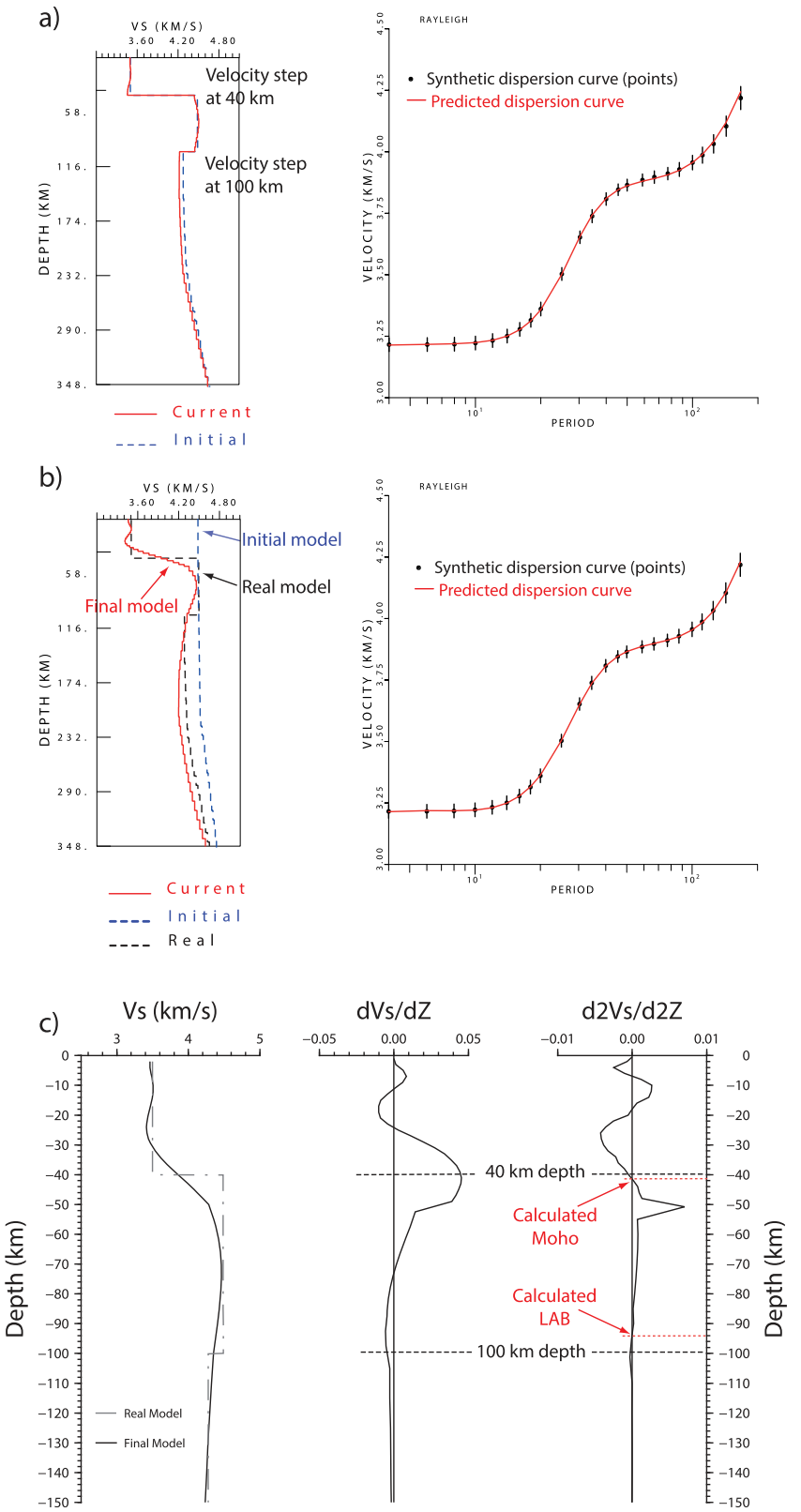

Figure 7. (a) 1-D model (dashed blue line) used to calculate the synthetic dispersion curve (dots). Red lines are the resulting 1-D shear velocity model and dispersion curve after inversion using as initial velocity model the one used to obtain the synthetic dispersion curve (blue dashed line). (b) Inversion of the synthetic dispersion curve using as initial Vs the model used with the real data. (c) First and second derivative of the final model after inversion in Figure 7b. We see that the Moho and LAB depth recovered have a discrepancies of about 2 and 6 km for the Moho and LAB, respectively.

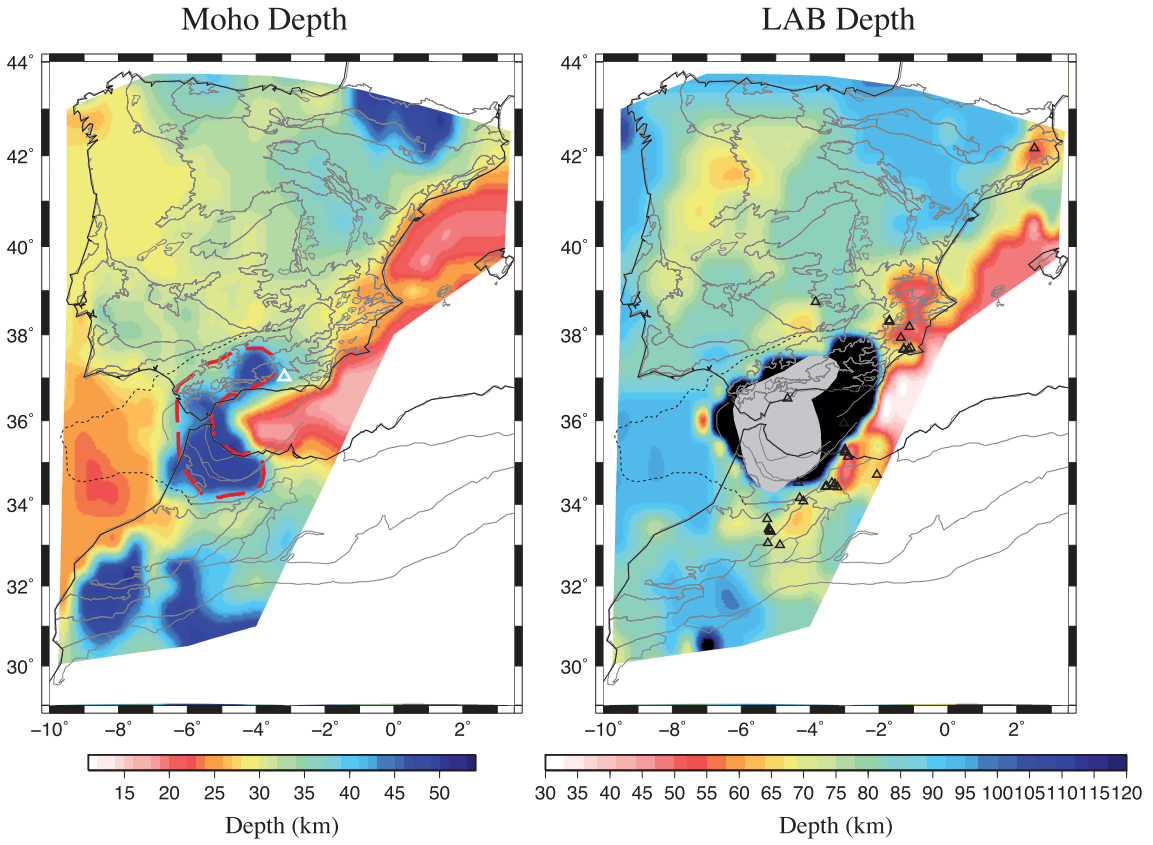

Figure 8. (a) Calculated crustal and (b) lithospheric thicknesses. (a) Red dashed line and (b) gray area indicate the shape of the high-velocity body at 60 and 90 km depth, respectively. Black area corresponds to the region where no LAB can be picked due to the presence of the Alboran Slab. The area with no ray coverage (see Figure 3b) is masked. White triangle (a) indicates the position of the Sierra Nevada, and black triangles (b) indicate the position of volcanics.

The lithospheric thickness varies throughout the study region (Figure 8b). Beneath the Pyrenees, the Ebro Basin, and the Iberian Chain the LAB is at ∼95 km depth. It shallows to ∼70 km at the western border of the Duero Basin and in the CIZ. Central Iberia has a lithospheric thickness of ∼ 82 km. Thinner lithosphere is observed in an area that extends from the eastern end of the Betics (the Prebetics) to Mallorca. Here the LAB is mapped as shallow as 50 km. The same lithospheric thickness is observed in the northeastern edge of Iberia, beneath the Catalan volcanic province. Beneath the Calatrava volcanic field, north of the Betics, the LAB is shallower than 70 km depth. Thin lithosphere (<85 km) is observed in the area around the Gibraltar Arc, surrounding the high shear velocity western Mediterranean slab [*Palomeras et al.*, 2014]. Due to the presence of the sinking western Mediterranean slab the LAB could not be picked in the Alboran region (black area in Figure 8b).

6. Discussion

In the following, we discuss first the results for the Iberian Massif. Then, we present an analysis of results within the areas affected by the deformation of northeastern Iberia. Finally, the tectonically active regions of the south, the Gibraltar arc region (Betics, Rif, and Alboran Sea), and the Atlas Mountains are presented.

6.1. Iberian Massif

The shear velocity model shows higher values throughout most of the crust of the Variscan domain, i.e., the Iberian Massif, than in the Alpine domain (Figures 5 and 6), particularly in the uppermost crust (5 km), and in the lower crust (25 km and deeper). The high crustal shear-wave velocities in the Iberian Massif correspond to metamorphic Paleozoic and Precambrian rocks that have been relatively undeformed since the Carboniferous.

The crustal thickness is dramatically different between Variscan Iberia, and Alpine Iberia being 31–35 km in the former, and 30–50 km in the latter. Modest crustal thickness variations exist within the Iberian Massif. The crust is 28–29 km thick in northwestern Iberia beneath the CIZ, thickening to 31–32 km to the east, near the Alpine Central System. Some authors suggest that crustal thinning in the CIZ resulted from extensional collapse of a thickened crust lying at the core of the orogen late in the Variscan orogeny [*Martínez Catalán et al*., 2014]. The extensional event is associated with melting of the lower crust, emplacement of granitoids, and widespread high-T low-P metamorphism, reequilibrating the crust and defining a new Moho [*Ayarza and Martínez Catalán*, 2007; *Martínez Catalán et al*., 2014]. Away from this core, the crust thickens to 31–32 km to the south of the Iberian Massif (Figure 8a) and to east, in the Cantabrian Mountains (West Asturian-Leonese Zone). In the southern part of the Iberian Massif, crustal shortening and thickening are not reported to be as important as in the northwest [*Simancas et al*., 2003], therefore post-Variscan melting and reequilibration did not take place leaving a slightly thicker crust. The crustal thickness values obtained in this work agree with those observed by vertical incidence and wide-angle experiments [*Simancas et al*., 2003; *Ayarza et al*., 2004; *Palomeras et al*., 2009; *Martínez Poyatos et al*., 2012; *Ehsan et al*., 2015].

Except the Betics and Valencia trough, northwestern Iberia also has low upper mantle shear-wave velocities and a thin lithosphere (<70 km, Figure 8b) compared to the rest of Iberia. There, upper mantle shear velocity is 6.5% lower than that of the southern Iberian Massif. In addition, this region has also a low *P* wave velocity anomaly in the shallow mantle [*Amaru*, 2007]. The possibility that the upper mantle was involved on the late Variscan thermal event described above cannot be ruled out. But in that case, we would expect that the lithospheric thickness would already have equilibrated. This suggests that this feature is the result of modern tectonics. Measured heat flow in the area are higher than those of a stable continent (>100 mW m^{-2}, reaching values over 150 mW m^{-2}) [*Fernàndez et al*., 1995] that the authors associate with water circulation through deep faults. The variations in surface heat flow beneath stable continents could be attributed to heat flow variations in the crustal heat production or to lithospheric thickness variations [*Pollack and Chapman*, 1977; *Artemieva*, 2009; *Petrunin et al*., 2013]. Thinner lithosphere implies larger temperature gradients and higher heat flow in the mantle lithosphere. This also involves an increase in temperature that translates into lower velocities. A reduction in shear-wave velocity of 6.5% corresponds to an increase in temperature of ~300 K [*Cammarano et al*., 2003]. Our results could thus indicate that a mantle source is producing the high heat flow values due to the thin lithosphere, although ours is the only evidences of an anomalously shallow asthenosphere in the area.

6.2. Northeastern Iberia

In this section, we discuss the results for the Pyrenees, Cantabrian Mountains, Iberian Chain, and Valencia Trough. The upper and lower crust shear-wave velocities in the Alpine domain are markedly lower than in the Variscan domain (Figure 5). The former are, usually, Mesozoic sediments deformed during the Alpine orogeny. The midcrust here is composed of the same Paleozoic basement that crops out on the Iberian Massif, with the result that midcrustal (~15 km) shear velocities are constant across the north half and west of Iberia. At lower crustal depths (>20 km), shear velocities beneath the Alpine Mountains (Pyrenees, Iberian Chain, Betics, Rif, and Atlas) are lower than beneath the Variscan domain due to Alpine crustal thickening. This pattern is also seen in the P-wave velocities from active seismic profiles in Iberia [*Díaz and Gallart*, 2009].

Thick crust (> 45 km) is observed beneath the western and central Pyrenees, similar to estimates from reflection profiles [*Choukroune and ECORS Team*, 1989]. The crust thins to the east to ~26 km at the Mediterranean coast. Away from the Pyrenees, to the west, the crust thins to ~33 km, then thickens to ~36–37 km beneath the Cantabrian Mountains. To the south the crust under the Iberian Chain is ~38 km thick.

The lithosphere is ~90 km deep under the Pyrenees and Iberian Chain and thins eastward and southward under the Mediterranean, reaching a minimum thickness of ~50 km under the southern Valencia Trough. Magnetotelluric profiling in the Pyrenees [*Campanyà et al*., 2012], give similar thicknesses whereas potential field modeling [*Zeyen and Fernàndez*, 1994], and seismic and geochemical data modeling [*Carballo et al*., 2014] image a thicker lithosphere (>120 km thick). These modeling studies extend through the Valencia Trough where the LAB thins to ~70 km. Our Moho depth indicates a rapid thinning from ~29 km in the Iberian margin up to ~18 km in the Valencia Trough in a short horizontal distance. Active seismic profiles across the continental margin and along the trough report similar crustal thickness changes

[*Gallart et al*., 1994]. The Valencia trough opened as a result of back-arc extension during the Alboran trench retreat (Oligocene), causing the thinning of the crust and lithosphere of the Iberian continental margin.

6.3. Alboran and Atlas Region

The actively deforming Gibraltar Arc has low crustal shear velocities at all depths and thicker crust than anywhere else in the study region. At the surface, this region corresponds to flysch units consisting of unmetamorphosed deep marine Meso-Cenozoic sediments, underlain by oceanic crust and/or thinned continental crust [*Sopeña*, 2004]. Low *P* wave velocities have been reported for the western Betics by *Barranco et al*. [1990]. At lower crustal depths (>20 km), the shear velocities beneath the Betics, Rif, and Atlas are lower than beneath the Variscan domain and are comparable to those in other Alpine belts in the region.

We observe unusually thick crust (∼50 km) under the western Betics and Rif, as reported previously in surface wave, receiver function, and active source investigations [*Mancilla et al*., 2012; *Gil et al*., 2014; *Palomeras et al*., 2014; *Thurner et al*., 2014]. The deep Moho around the western Alboran Sea is coincident with the high shear velocity anomaly of the Alboran slab (Figures 6 and 8a, red dashed line). Interpretation of receiver functions events at the base of the crust [*Thurner et al*., 2014] suggests that lithospheric delamination is ongoing and is now removing the continental lower crust beneath the Gibraltar arc from east to west, and is depressing the base of the crust prior to delamination (Figure 6). We also observe that the continental margins adjacent to the Gibraltar Arc to the north (eastern Pre-Betics), northeast (Valencia Trough), and south (Rif) have thinner crust and lithosphere than would be expected for passive margins (Figure 8b). We attribute this to viscous removal of the bottom of the lithosphere by the descending Alboran plate [*Tao and O'Connell*, 1992; *Levander et al*., 2014].

Recent 3-D geodynamic modeling [*Chertova et al*., 2014] reconstructs the evolution of the Alboran slab starting with NW-directed subduction along the Balearic margin around ∼35 Ma, and trench retreat to the African margin in the Middle Miocene. In the late Tortonian (7–8 Ma), the Alboran slab rotated >90° moving westward with the Algerian Basin opening behind it, reaching its current position in the Gibraltar Arc. This evolution is consistent with the geochemistry of igneous rocks in the southern Iberian and northern Moroccan margins, which evolves from Si-K-rich to Si-poor between 6.3 and 4.8 Ma (Messinian to Early Pliocene) [*Duggen et al*., 2004]. Before the Messinian, the volcanic signature (Si-rich basalts) is related to subduction whereas the post-Messinian volcanism (Si-poor basalts) is related to upwelling asthenosphere due to removal of subcontinental lithosphere [*Duggen et al*., 2005; *Levander et al*., 2014]. The age of these volcanics decreases to the west in the same sense as slab retreat and delamination of the adjacent continental lithosphere [*Levander et al*., 2014; *Thurner et al*., 2014]. Replacement of delaminating lithosphere by asthenosphere results in decompression melting (Figure 8b), the source of the Si-poor basalts. We observe an 8.5% reduction on the upper mantle shear velocities around the eastern Gibraltar arc relative to the rest of Iberia and Morocco, which can occur for 1% partial melt [*Hammond and Humphreys*, 2000].

The evolution of the subduction driven delamination is also expressed at the surface by the age of emergence of the marine sedimentary basins in Betics and Rif. In the easternmost Betics (Pre-Betics) basins started to emerge in late Miocene (∼11 Ma) and uplift progressed to the west [*Iribarren et al*., 2009]. Current uplift rates of 3 mm/yr have been reported in the eastern Betics [*Serpelloni et al*., 2013]. In the eastern Betics, where delamination has already occurred, the crust thins by up to 25 km (50%) and the lithosphere up to 50 km (Figure 8), and the load of the descending Alboran slab is removed. We conclude that the uplift is a transient phenomenon, a result of crustal and lithospheric delamination.

Our results confirm a relatively thin crust and shallow LAB beneath the Middle and High Atlas, with both crust and lithosphere thickening through the western Atlas. The Atlas Mountains present elevations over 4000 m but with modest amounts of shortening (15–30%) [*Beauchamp et al*., 1999; *Teixell et al*., 2003]. Several authors have suggested a thin lithosphere beneath the High and Middle Atlas to support its elevation and to explain the strong positive geoid anomaly [*Teixell et al*., 2003, 2005; *Ayarza et al*., 2005; *Zeyen et al*., 2005; *Fullea et al*., 2010]. Different processes have been proposed to explain the source of the shallow asthenosphere: (1) a mantle plume that is part of the Canary system [*Zeyen et al*., 2005; *Missenard et al*., 2006; *Duggen et al*., 2009; *Miller and Becker*, 2013; *Sun et al*., 2014; *Miller et al*., 2015], (2) lateral flow of asthenospheric mantle at the edge of the Alboran slab [*Teixell et al*., 2005], (3) flow caused by edge-driven convection [*Missenard and Cadoux*, 2012; *Kaislaniemi and van Hunen*, 2014], and (4) delamination of the local upper mantle beneath the High and Middle Atlas [*Bezada et al*., 2014]. All these processes result in a

thinner lithosphere. The low shear velocities we observe beneath the Atlas are consistent with any of these models. However, we find little evidence for a shallow asthenospheric channel to connect the Canaries mantle plume with the High Atlas [*Duggen et al*., 2009; *Miller and Becker*, 2013; *Miller et al*., 2015]. The LAB map shows that the thin lithosphere under the Middle and High Atlas appears connected to the thin lithosphere around the Rif Mountains suggesting that the thin lithosphere under the central Atlas is related to the Alboran subduction. *Levander et al*. [2014] suggest that the lithospheric thickness gradient between the West Africa Craton and delaminated lithosphere around the Gibraltar Arc slab is triggering secondary edge-driven convection centered beneath the High and Middle Atlas. The observed low upper mantle shear velocities would result from partial melt produced by decompression in the edge-driven convection cells [*Kaislaniemi and van Hunen*, 2014]. This would produce thermal erosion shallowing the LAB. It also explains the amount, and the spatial and temporal distribution of Cenozoic volcanism observed in the Atlas.

6.4. Other Low Upper Mantle Shear Velocities

In addition to volcanism related to the Gibraltar arc related to subduction and delamination [*Duggen et al*., 2005], there are two other Late Miocene-Late Pliocene volcanic fields in Iberia: the Calatrava Volcanic field (CVF) at the north of the Betics, and the Catalan Volcanic Province (CVP) in northeastern Iberia. Thin lithosphere is mapped beneath both sites with low upper mantle velocities (4.2 km/s) that we identify as asthenosphere at ~70 km depth and ~60 km depth at the CVF and the CVP, respectively. The lateral velocity contrast is approximately 8.5% for these volcanic fields. These variations in Vs are greater than those resulting from the transition from a dry depleted lithosphere to a hydrated, fertile asthenosphere, which range from ~1% to 2.5% [*Lee*, 2003; *Schutt and Lesher*, 2006]. To account for the observed shear velocity reduction (~8.5%) another source must be invoked. An increase in temperature of 450°K is needed to account the 8.5% velocity reduction [*Cammarano et al*., 2003]. We can also explain the observed Vs decrease with 1% partial melt [*Hammond and Humphreys*, 2000]. Any of those mechanisms or both combined would account for the Late Neogene magmatism identified in these areas.

7. Conclusion

We have developed a 3-D shear velocity model for Iberia and Morocco from inversion of phase velocities determined from ambient noise and teleseismic finite-frequency Rayleigh wave tomography. The model extends from the surface to ~200 km depth. From the model, we have inferred crustal and lithospheric thickness. Broadly speaking the shear velocities in the crust, crustal thickness, and lithospheric thickness are consistent with what is understood about western Mediterranean geologic history, and divide Iberia into Variscan (Iberian Massif), Alpine (Pyrenees, Cantabrian, and Iberian Chain Mountains), and currently deforming terranes (Gibraltar Arc). Similarly Morocco can be divided into cratonic terranes, Atlas Mountains and Gibraltar arc. At the crustal level, areas with Variscan basement outcrops (Iberian Massif and Moroccan Meseta) show higher shear velocity than areas affected by the Alpine orogeny. Modest differences in the Variscan terranes of the Iberian Massif can be attributed to differences in orogenic evolution.

The tectonically active Gibraltar arc has a thick crust (>50 km) that lies above the high shear velocity Alboran slab. The images and previous receiver function studies show that the slab is still attached to the western Betics and Rif Mountains, where the crust is thickest, but has delaminated from under the eastern Betics and Rif where the crust and the lithosphere are now thin. Surface uplift and geochemical signatures support the east to west subduction driven delamination of the lithosphere under the Betics and Rif. The High and Middle Atlas can be considered part of the Gibraltar arc system broadly defined, and have relatively thin crust (<40 km) and little to no mantle lithosphere, suggesting that the asthenosphere provides the buoyancy needed to support their high elevations. We have also identified likely mantle sources for the Late Miocene magmatism in the Calatrava field and the Catalan Volcanic Province.

Acknowledgments

This research was funded by the U.S. National Science Foundation EAR-0808939. The deployment of the IberArray broadband seismic network is part of the CONSOLIDER-Ingenio 2010 TOPO-IBERIA (CSD2006-00041: Geosciences in Iberia: Integrated studies on Topography and 4-D Evolution) grant from the Spanish Ministry of Science and Innovation. Additional funding was provided by the Spanish ministry under grants CGL2010-17280, CGL2006-01171, CGL2009-09727, and CGL2007-63889, and by Generalitat de Catalunya under grant 2009 SGR 6. We thank the IRIS data management center, the Instituto Geografico Nacional (Spain), the IPMA (Portugal), the Centro de Geofisica da Universidade de Lisboa (Portugal), the Universidad Complutense de Madrid (Spain), the ICGC, ROA, IAG, and the University of Muenster (Germany) for contributing data to this study. Thanks to the Seismology and Tectonics at Rice (STAR) group for valuable discussions. We also thanks to the anonymous reviewer and the editor for the comments that improved the manuscript.

References

Amaru, M. L. (2007), Global travel time tomography with 3-D reference models, PhD Thesis, Utrecht University, Netherlands.

Artemieva, I. M. (2009), The continental lithosphere: Reconciling thermal, seismic, and petrologic data, *Lithos*, *109*(1–2), 23–46, doi:10.1016/j.lithos.2008.09.015.

Ayarza, P., and J. R. Martínez Catalán (2007), Potential field constraints on the deep structure of the Lugo gneiss dome (NW Spain), *Tectonophysics*, *439*(1–4), 67–87, doi:10.1016/j.tecto.2007.03.007.

Ayarza, P., J. R. Martínez Catalán, J. Alvarez-Marrón, H. Zeyen, and C. Juhlin (2004), Geophysical constraints on the deep structure of a limited ocean-continent subduction zone at the North Iberian Margin, *Tectonics*, *23*, TC1010, doi:10.1029/2002TC001487.

Ayarza, P., F. Alvarez-Lobato, A. Teixell, M. L. Arboleya, E. Tesón, M. Julivert, and M. Charroud (2005), Crustal structure under the central High Atlas Mountains (Morocco) from geological and gravity data, *Tectonophysics*, *400*(1–4), 67–84, doi:10.1016/j.tecto.2005.02.009.

Ayarza, P., et al. (2014), Crustal thickness and velocity structure across the Moroccan Atlas from long offset wide-angle reflection seismic data: The SIMA experiment, *Geochem. Geophys. Geosyst.*, *15*, 1698–1717, doi:10.1002/2013GC005164.

Barmin, M. P., M. H. Ritzwoller, and A. L. Levshin (2001), A fast and reliable method for surface wave tomography, *Pure Appl. Geophys.*, *158*(8), 1351–1375, doi:10.1007/PL00001225.

Barranco, L. M., J. Ansorge, and E. Banda (1990), Seismic refraction constraints on the geometry of the Ronda peridotitic massif (Betic Cordillera, Spain), *Tectonophysics*, *184*, 379–392.

Beauchamp, W., R. W. Allmendinger, M. Barazangi, A. Demnati, M. El Alji, and M. Dahmani (1999), Inversion tectonics and the evolution of the High Atlas Mountains, Morocco, based on a geological-geophysical transect, *Tectonics*, *18*(2), 163–184.

Bensen, G. D., M. H. Ritzwoller, M. P. Barmin, A. L. Levshin, F. Lin, M. P. Moschetti, N. M. Shapiro, and Y. Yang (2007), Processing seismic ambient noise data to obtain reliable broad-band surface wave dispersion measurements, *Geophys. J. Int.*, *169*(3), 1239–1260, doi:10.1111/j.1365-246X.2007.03374.x.

Bezada, M. J., E. D. Humphreys, D. R. Toomey, M. Harnafi, and J. M. Davila (2013), Evidence for slab rollback in westernmost Mediterranean from improved upper mantle imaging, *Earth Planet. Sci. Lett.*, *368*, 51–60.

Bezada, M. J., E. D. Humphreys, J. M. Davila, R. Carbonell, M. Harnafi, I. Palomeras, and A. Levander (2014), Piecewise delamination of Moroccan lithosphere from beneath the Atlas Mountains, *Geochem. Geophys. Geosystems*, *15*, 975–985, doi:10.1002/2013GC005059.

Blanco, M. J., and W. Spakman (1993), The P-wave velocity structure of the mantle below the Iberian Peninsula: Evidence for subducted lithosphere below southern Spain, *Tectonophysics*, *221*, 13–34.

Bosch, D., R. C. Maury, M. El Azzouzi, C. Bollinger, H. Bellon, and P. Verdoux (2014), Lithospheric origin for Neogene-Quaternary Middle Atlas lavas (Morocco): Clues from trace elements and Sr-Nd-Pb-Hf isotopes, *Lithos*, *205*, 247–265, doi:10.1016/j.lithos.2014.07.009.

Buforn, E., and A. Udias (2010), Azores-tunisia, a tectonically complex plate boundary, *Adv. Geophys.*, *52*, 139–182.

Buforn, E., A. Udias, and R. Madariaga (1991), Intermediate and deep earthquakes in Spain, *Pure Appl. Geophys.*, *136*(4), 375–393.

Calvert, A., E. Sandvol, D. Seber, M. Barazangi, S. Roecker, T. Mourabit, F. Vidal, G. Alguacil, and N. Jabour (2000), Geodynamic evolution of the lithosphere and upper mantle beneath the Alboran region of the western Mediterranean: Constraints from travel time tomography, *J. Geophys. Res.*, *105*(B5), 10,871–10,898.

Cammarano, F., S. Goes, P. Vacher, and D. Giardini (2003), Inferring upper-mantle temperatures from seismic velocities, *Phys. Earth Planet. Inter.*, *138*(3–4), 197–222, doi:10.1016/S0031-9201(03)00156-0.

Campanyà, J., J. Ledo, P. Queralt, A. Marcuello, M. Liesa, and J. A. Muñoz (2012), New geoelectrical characterisation of a continental collision zone in the West-Central Pyrenees: Constraints from long period and broadband magnetotellurics, *Earth Planet. Sci. Lett.*, *333–334*, 112–121, doi:10.1016/j.epsl.2012.04.018.

Carballo, A., M. Fernandez, M. Torné, I. Jiménez-Munt, and A. Villaseñor (2014), Thermal and petrophysical characterization of the lithospheric mantle along the northeastern Iberia geo-transect, *Gondwana Res.*, *27*, 1430–1445, doi:10.1016/j.gr.2013.12.012.

Cebriá, J.-M., and J. López-Ruiz (1995), Alkali basalts and leucitites in an extensional intracontinental plate setting: The late Cenozoic Calatrava Volcanic Province (central Spain), *Lithos*, *35*(1–2), 27–46, doi:10.1016/0024-4937(94)00027-Y.

Chertova, M. V., W. Spakman, T. Greenen, A. P. van den Berg, and D. J. J. van Hinsbergen (2014), Underpinning tectonic reconstructions of the western Mediterranean region with dynamic slab evolution from 3-D numerical modeling, *J. Geophys. Res. Solid Earth*, *119*, 5876–5902, doi:10.1002/2014JB011150.

Choukroune, P., and ECORS Team (1989), The ECORS Pyrenean deep seismic profile reflection data and the overall structure of an Orogenic Belt, *Tectonics*, *8*(1), 23–39.

Díaz, J., and J. Gallart (2009), Crustal structure beneath the Iberian Peninsula and surrounding waters: A new compilation of deep seismic sounding results, *Phys. Earth Planet. Inter.*, *173*(1–2), 181–190, doi:10.1016/j.pepi.2008.11.008.

Díaz, J., A. Villaseñor, J. Gallart, J. Morales, A. Pazos, D. Cordoba, J. A. Pulgar, J. L. García Lobón, M. Harnafi, and T. S. W. Group (2009), The IBERARRAY broadband seismic network: A new tool to investigate the deep structure beneath Iberia, *Orfeus Newsl.*, *8*(2), 1–6.

Duggen, S., K. Hoernle, P. van den Bogaard, and C. Harris (2004), Magmatic evolution of the Alboran region: The role of subduction in forming the western Mediterranean and causing the Messinian Salinity Crisis, *Earth Planet. Sci. Lett.*, *218*(1–2), 91–108, doi:10.1016/S0012-821X(03)00632-0.

Duggen, S., K. Hoernle, P. van den Bogaard, and D. Garbe-Schonberg (2005), Post-collisional transition from subduction- to intraplate-type magmatism in the Westernmost Mediterranean: Evidence for continental-edge delamination of subcontinental lithosphere, *J. Petrol.*, *46*(6), 1155–1201, doi:10.1093/petrology/egi013.

Duggen, S., K. A. Hoernle, F. Hauff, A. Klugel, M. Bouabdellah, and M. F. Thirlwall (2009), Flow of Canary mantle plume material through a subcontinental lithospheric corridor beneath Africa to the Mediterranean, *Geology*, *37*(3), 283–286, doi:10.1130/G25426A.1.

Eaton, D. W., F. Darbyshire, R. L. Evans, H. Grütter, A. G. Jones, and X. Yuan (2009), The elusive lithosphere-asthenosphere boundary (LAB) beneath cratons, *Lithos*, *109*(1–2), 1–22, doi:10.1016/j.lithos.2008.05.009.

Ehsan, S. A., R. Carbonell, P. Ayarza, D. Martí, D. Martínez Poyatos, J. F. Simancas, A. Azor, C. Ayala, M. Torné, and A. Pérez-Estaún (2015), Lithospheric velocity model across the Southern Central Iberian Zone (Variscan Iberian Massif): The ALCUDIA wide-angle seismic reflection transect, *Tectonics*, *34*, 535–554, doi:10.1002/2014TC003661.

Fernàndez, M., C. Almeida, and J. Cabal (1995), Heat flow and heat production in western Iberia, in *World Geothermal Congress*, edited by E. Barbier, pp. 745–749, International Geotherma Association, Florence.

Forsyth, D. W., and A. Li (2005), Array-analysis of Two-dimensional Variations in surface wave phase velocity and azimuthal anisotropy in the presence of multipathing interference, in *Seismic Earth: Array Analysis of Broadband Seismograms*, edited by A. Levander and G. Nolet, pp. 81–97, AGU, Washington, D. C.

Fullea, J., M. Fernàndez, J. C. Afonso, J. Vergés, and H. Zeyen (2010), The structure and evolution of the lithosphere-asthenosphere boundary beneath the Atlantic-Mediterranean Transition Region, *Lithos*, *120*(1–2), 74–95, doi:10.1016/j.lithos.2010.03.003.

Gallart, J., N. Vidal, and J.. Danobeitia (1994), Lateral variations in the deep crustal structure at the Iberian margin of the Valencia trough imaged from seismic reflection methods, *Tectonophysics*, *232*, 59–75, doi:10.1016/0040-1951(94)90076-0.

Garcia-Castellanos, D., and A. Villaseñor (2011), Messinian salinity crisis regulated by competing tectonics and erosion at the Gibraltar arc, *Nature*, *480*(7377), 359–63, doi:10.1038/nature10651.

Gibbons, W., and T. Moreno (Eds.) (2002), *The Geology of Spain*, Geol. Soc., London, U. K.

Gil, A., J. Gallart, J. Díaz, R. Carbonell, M. Torné, A. Levander, and M. Harnafi (2014), Crustal structure beneath the Rif Cordillera, North Morocco, from the RIFSIS wide-angle reflection seismic experiment, *Geochem. Geophys. Geosyst.*, *15*, 4712–4733, doi:10.1002/2014GC005485.

Gutscher, M.-A., J. Malod, J.-P. Rehault, I. Contrucci, F. Klingelhoefer, L. Mendes-Victor, and W. Spakman (2002), Evidence for active subduction beneath Gibraltar, *Geology*, *30*(12), 1071–1074, doi:10.1130/0091-7613(2002)030 < 1071.

Hammond, W. C., and E. D. Humphreys (2000), Upper mantle seismic wave velocity: Effects of realistic partial melt geometries, *J. Geophys. Res.*, *105*(B5), 10,975–10,986, doi:10.1029/2000JB900041.

Herrmann, R. B. (2013), Computer programs in seismology: An evolving tool for instruction and research, *Seismol. Res. Lett.*, *84*(6), 1081–1088, doi:10.1785/0220110096.

Iribarren, L., J. Vergés, and M. Fernàndez (2009), Sediment supply from the Betic–Rif orogen to basins through Neogene, *Tectonophysics*, *475*(1), 68–84, doi:10.1016/j.tecto.2008.11.029.

Jacobshagen, V., K. Gorler, and P. Giese (1988), Geodynamic evolution of the Atlas System (Morocco) in post-Palaeozoic times, in *The Atlas System of Morocco: Studies on Its Geodynamic Evolution, Lecture Notes Earth Sci.*, edited by V. Jacobshagen, pp. 481–499, Springer, New York.

Kaislaniemi, L., and J. van Hunen (2014), Dynamics of lithosphere thinning and mantle melting by edge-driven convection: Application to Moroccan Atlas mountains, *Geochem. Geophys. Geosyst.*, *15*, 3175–3189, doi:10.1002/2014GC005414.

Kennett, B. L. N., E. R. Engdah, and R. Buland (1995), Constraints on seismic velocities in the Earth from traveltimes, *Geophys. J. Int.*, *122*, 108–124.

Koulali, A., D. Ouazar, A. Tahayt, R. W. King, P. Vernant, R. E. Reilinger, S. McClusky, T. Mourabit, J. M. Davila, and N. Amraoui (2011), New GPS constraints on active deformation along the Africa-Iberia plate boundary, *Earth Planet. Sci. Lett.*, *308*(1–2), 211–217, doi:10.1016/j.epsl.2011.05.048.

Laville, E., A. Pique, M. Amrhar, and M. Charroud (2004), A restatement of the Mesozoic Atlasic Rifting (Morocco), *J. Afr. Earth Sci.*, *38*, 145–153, doi:10.1016/j.jafrearsci.2003.12.003.

Lee, C.-T. A. (2003), Compositional variation of density and seismic velocities in natural peridotites at STP conditions: Implications for seismic imaging of compositional heterogeneities in the upper mantle, *J. Geophys. Res.*, *108*(B9), 2441, doi:10.1029/2003JB002413.

Levander, A. et al. (2014), Subduction-driven recycling of continental margin lithosphere, *Nature*, *515*(7526), 253–256, doi:10.1038/nature13878.

Levshin, A., L. Ratnikova, and J. Berger (1992), Peculiarities of surface-wave propagation across central Eurasia, *Bull. Seismol. Soc. Am.*, *82*(6), 2464–2493.

Li, A., D. W. Forsyth, and K. M. Fischer (2003), Shear velocity structure and azimuthal anisotropy beneath eastern North America from Rayleigh wave inversion, *J. Geophys. Res.*, *108*(B8), 2362, doi:10.1029/2002JB002259.

Mancilla, F. D. L. et al. (2012), Crustal thickness variations in northern Morocco, *J. Geophys. Res.*, *117*, B02312, doi:10.1029/2011JB008608.

Martí, J., J. Mitjavila, E. Roca, and A. Aparicio (1992), Cenozoic magmatism of the valencia trough (western mediterranean): Relationship between structural evolution and volcanism, *Tectonophysics*, *203*(1–4), 145–165, doi:10.1016/0040-1951(92)90221-Q.

Martínez Catalán, J. R., F. J. Rubio Pascual, A. Diez Montes, R. Diez Fernandez, J. Gomez Barreiro, I. Dias Da Silva, E. Gonzalez Clavijo, P. Ayarza, and J. E. Alcock (2014), The late Variscan HT/LP metamorphic event in NW and Central Iberia: Relationships to crustal thickening, extension, orocline development and crustal evolution, in *The Variscan Orogeny: Extent, Timescale and the Formation of the European Crust*, vol. 405, edited by K. Schulmann et al., pp. 225–247, Geol. Soc., Spec. Publ., London, U. K.

Martínez Poyatos, D., et al. (2012), Imaging the crustal structure of the Central Iberian Zone (Variscan Belt): The ALCUDIA deep seismic reflection transect, *Tectonics*, *31*, TC3017, doi:10.1029/2011TC002995.

Matte, P. (1986), Tectonic and plate tectonics model for the Variscan belt of Europe, *Tectonophysics*, *126*, 329–374.

Matte, P. (2001), The Variscan collage and orogeny (480–290 Ma) and the tectonic definition of the Armorica microplate: A review, *Terra Nov.*, *13*, 122–128.

Miller, M. S., and T. W. Becker (2013), Reactivated lithospheric-scale discontinuities localize dynamic uplift of the Moroccan Atlas Mountains, *Geology*, *42*(1), 35–38, doi:10.1130/G34959.1.

Miller, M. S., L. J. O'Driscoll, A. J. Butcher, and C. Thomas (2015), Imaging Canary Island hotspot material beneath the lithosphere of Morocco and southern Spain, *Earth Planet. Sci. Lett.*, *431*, 186–194, doi:10.1016/j.epsl.2015.09.026.

Missenard, Y., and A. Cadoux (2012), Can Moroccan Atlas lithospheric thinning and volcanism be induced by Edge-Driven Convection?, *Terra Nov.*, *24*, 27–33, doi:10.1111/j.1365-3121.2011.01033.x.

Missenard, Y., H. Zeyen, D. Frizon de Lamotte, P. Leturmy, C. Petit, M. Sébrier, and O. Saddiqi (2006), Crustal versus asthenospheric origin of relief of the Atlas Mountains of Morocco, *J. Geophys. Res.*, *111*, B03401, doi:10.1029/2005JB003708.

Mitchell, B. J. (1995), Anelastic structure and evolution of the continental crust and upper mantle from seismic surface wave attenuation, *Rev. Geophys.*, *33*(4), 441–462.

Palomeras, I., R. Carbonell, I. Flecha, F. Simancas, P. Ayarza, J. Matas, D. Martínez Poyatos, A. Azor, F. González-Lodeiro, and A. Pérez-Estaún (2009), Nature of the lithosphere across the Variscan orogen of SW Iberia: Dense wide-angle seismic reflection data, *J. Geophys. Res.*, *114*, B02302, doi:10.1029/2007JB005050.

Palomeras, I., S. Thurner, A. Levander, K. Liu, A. Villaseñor, R. Carbonell, and M. Harnafi (2014), Finite-frequency Rayleigh wave tomography of the western Mediterranean: Mapping its lithospheric structure, *Geochem. Geophys. Geosyst.*, *15*, 140–160, doi:10.1002/2013GC004861.

Petrunin, A. G., I. Rogozhina, A. P. M. Vaughan, I. T. Kukkonen, M. K. Kaban, I. Koulakov, and M. Thomas (2013), Heat flux variations beneath central Greenland's ice due to anomalously thin lithosphere, *Nat. Geosci.*, *6*(9), 746–750, doi:10.1038/ngeo1898.

Pollack, N., and S. Chapman (1977), On the regional variation of heat flow, geotherms, and lithospheric thickness, *Tectonophysics*, *38*, 279–296.

Priestley, K., and E. Debayle (2003), Seismic evidence for a moderately thick lithosphere beneath the Siberian Platform, *Geophys. Res. Lett.*, *30*(3), 1118, doi:10.1029/2002GL015931.

Rosenbaum, G., G. S. Lister, and C. Duboz (2002), Reconstruction of the tectonic evolution of the western Mediterranean since the Oligocene, *J. Virtual Explor.*, *8*, 107–130.

Royden, L. H. (1993), Evolution of retreating subduction boundaries formed during continental collision, *Tectonics*, *12*(3), 629–638.

Schutt, D. L., and C. E. Lesher (2006), Effects of melt depletion on the density and seismic velocity of garnet and spinel lherzolite, *J. Geophys. Res.*, *111*, B05401, doi:10.1029/2003JB002950.

Serpelloni, E., C. Faccenna, G. Spada, D. Dong, and S. D. P. Williams (2013), Vertical GPS ground motion rates in the Euro-Mediterranean region: New evidence of velocity gradients at different spatial scales along the Nubia-Eurasia plate boundary, *J. Geophys. Res. Solid Earth*, *118*, 6003–6024, doi:10.1002/2013JB010102.

Silveira, G., N. Afonso Dias, and A. Villaseñor (2013), Seismic imaging of the western Iberian crust using ambient noise: Boundaries and internal structure of the Iberian Massif, *Tectonophysics*, *589*, 186–194, doi:10.1016/j.tecto.2012.12.025.

Simancas, J. F., et al. (2003), Crustal structure of the transpressional Variscan orogen of SW Iberia: SW Iberia deep seismic reflection profile (IBERSEIS), *Tectonics*, *22*(6), 1062, doi:10.1029/2002TC001479.

Sopeña, A. (2004), Cordillera Bética y Baleares, in *Geología de España*, edited by J. A. Vera, pp. 347–464, Inst. Geol. y Minero Espanol, Madrid.

Stich, D., E. Serpelloni, F. D. L. Mancilla, and J. Morales (2006), Kinematics of the Iberia–Maghreb plate contact from seismic moment tensors and GPS observations, *Tectonophysics*, *426*(3–4), 295–317, doi:10.1016/j.tecto.2006.08.004.

Sun, D., M. S. Miller, A. F. Holt, and T. W. Becker (2014), Hot upwelling conduit beneath the Atlas Mountains, Morocco, *Geophys. Res. Lett.*, *41*, 8037–8044, doi:10.1002/2014GL061884.

Tao, W. C., and R. O'Connell (1992), Ablative subduction: A two-sided subduction alternative model to the conventional, *J. Geophys. Res.*, *97*(B6), 8877–8904.

Teixell, A., M. L. Arboleya, M. Julivert, and M. Charroud (2003), Tectonic shortening and topography in the central High Atlas (Morocco), *Tectonics*, *22*(5), 1051, doi:10.1029/2002TC001460.

Teixell, A., P. Ayarza, H. Zeyen, M. Fernandez, and M.-L. Arboleya (2005), Effects of mantle upwelling in a compressional setting: The Atlas Mountains of Morocco, *Terra Nov.*, *17*(5), 456–461, doi:10.1111/j.1365-3121.2005.00633.x.

Thurner, S., I. Palomeras, A. Levander, R. Carbonell, and C.-T. Lee (2014), Ongoing lithospheric removal in the western Mediterranean: Evidence from Ps receiver functions and thermobarometry of Neogene basalts (PICASSO project), *Geochem. Geophys. Geosyst.*, *15*, 1113–1127, doi:10.1002/2013GC005124.

Van Hinsbergen, D. J. J., R. L. M. Vissers, and W. Spakman (2014), Origin and consequences of western Mediterranean subduction, rollback, and slab segmentation, *Tectonics*, *33*, 393–419, doi:10.1002/2013TC003349.

Yang, Y., and D. W. Forsyth (2006), Regional tomographic inversion of the amplitude and phase of Rayleigh waves with 2-D sensitivity kernels, *Geophys. J. Int.*, *166*(3), 1148–1160, doi:10.1111/j.1365-246X.2006.02972.x.

Yao, H., C. Beghein, and R. D. van der Hilst (2008), Surface wave array tomography in SE Tibet from ambient seismic noise and two-station analysis—II: Crustal and upper-mantle structure, *Geophys. J. Int.*, *173*(1), 205–219, doi:10.1111/j.1365-246X.2007.03696.x.

Zeyen, H., and M. Fernàndez (1994), Integrated lithospheric modeling combining thermal, gravity and local isostasy analysis: Application to the NE Spanish Geotransect, *J. Geophys. Res.*, *99*(B9), 18,089–18,102.

Zeyen, H., P. Ayarza, M. Fernàndez, and A. Rimi (2005), Lithospheric structure under the western African-European plate boundary: A transect across the Atlas Mountains and the Gulf of Cadiz, *Tectonics*, *24*, TC2001, doi:10.1029/2004TC001639.